Vibrational thermodynamics of $Fe_{90}Zr_7B_3$ nanocrystalline alloy from nuclear inelastic scattering

S. Stankov,[1,2,*] M. Miglierini,[3,4] A. I. Chumakov,[5] I. Sergueev,[5] Y. Z. Yue,[6,7] B. Sepiol,[8] P. Svec,[9] L. Hu,[6,7] and R. Rüffer[5]

[1]*Institute for Synchrotron Radiation, Karlsruhe Institute of Technology, Campus Nord, 76344 Eggenstein-Leopoldshafen, Germany*
[2]*Laboratory for Applications of Synchrotron Radiation, Karlsruhe Institute of Technology, Campus Süd, 76131 Karlsruhe, Germany*
[3]*Department of Nuclear Physics and Technology, Slovak University of Technology, 81219 Bratislava, Slovakia*
[4]*Center for Nanomaterials Research, Palacky University, 77146 Olomouc, Czech Republic*
[5]*European Synchrotron Radiation Facility, BP 220, 38043 Grenoble, France*
[6]*Section of Chemistry, Aalborg University, 9000 Aalborg, Denmark*
[7]*Key Laboratory of Liquid Structure and Heredity of Materials, Shandong University, 250061 Jinan, China*
[8]*Faculty of Physics, University of Vienna, 1090 Vienna, Austria*
[9]*Institute of Physics, Slovak Academy of Sciences, 84511 Bratislava, Slovakia*

(Received 19 July 2010; published 5 October 2010)

Recently we determined the iron-partial density of vibrational states (DOS) of nanocrystalline $Fe_{90}Zr_7B_3$ (Nanoperm), synthesized by crystallization of an amorphous precursor, for various stages of nanocrystallization separating the DOS of the nanograins from that of the interfaces [S. Stankov, Y. Z. Yue, M. Miglierini, B. Sepiol, I. Sergueev, A. I. Chumakov, L. Hu, P. Svec, and R. Rüffer, Phys. Rev. Lett. **100**, 235503 (2008)]. Here we present quantitative analysis of the evolution of various thermoelastic properties calculated from DOS such as mean-force constant, mean atomic displacement, vibrational entropy, and lattice specific heat as the material transforms from amorphous, through nanocrystalline, to fully crystallized state. The reported results shed new light on the previously observed anomalies in the vibrational thermodynamics of nanocrystalline materials.

DOI: 10.1103/PhysRevB.82.144301 PACS number(s): 65.80.−g, 63.22.−m, 63.50.−x, 76.80.+y

I. INTRODUCTION

The vibrational thermodynamics[1] of nanocrystalline (NC) materials[2] has attracted a considerable interest mainly due to the observed anomalies in the vibrational entropy and lattice specific heat. Room-temperature enhancements of the vibrational entropy of $0.019k_B$/atom (Ref. 3) for NC Fe prepared by ball milling and of $0.01k_B$/atom (Ref. 4) for NC Fe synthesized by ballistic consolidation, were reported. For NC Ni_3Fe a deviation of up to $0.2k_B$/atom from the bulk value was observed.[5,6] In theoretical calculations an enhancement of $0.1k_B$/atom was obtained for Ag nanoparticles[7] while for NC Fe and Ni_3Fe the corresponding values are $0.215k_B$/atom and $0.15k_B$/atom.[8]

Similarly to the vibrational entropy, an enhancement of the lattice specific heat has also been detected. Deviations at room temperature ranging from 2% for NC Se,[9] 3% for NC Ni,[10] 10% for NC Cu,[11] 20% for NC Ru (Ref. 12) and NC Pt,[13] and 40% for NC Pd (Ref. 11) relative to the bulk values were reported. The increase in the specific heat has also been theoretically confirmed for a model NC system.[14]

All these anomalies reflect the well-known anomalies of the density of vibrational states (DOS) observed for various NC materials. The common features are enhancement of the DOS at low and high energies and broadening of the phonon peaks.[3–6,15–24] The thorough understanding of the origin of these anomalies, however, requires disentangling the effects of disorder, reduced size, and chemical state (i.e., oxidation) on the vibrational DOS as well as proper accounting for the presence of pores and voids, and internal surfaces, which is a complex and demanding task.

Recently, the DOS of the nanograins and the interfaces was determined[25] for various grain sizes and interface thicknesses of NC $Fe_{90}Zr_7B_3$ (Nanoperm) prepared by crystallization of an amorphous (AM) precursor. This sample preparation technique was selected among the other methods due to the following considerations: (i) the NC materials exhibit homogenous, porosity free, and dense interfaces. This allows for ruling out the contribution of the free volumes to the vibrational thermodynamics of the NC materials. (ii) The isothermal annealing of an amorphous Fe *M*B (*M* stands for Nb, Zr, or Hf) alloy leads to two steps of crystallization.[26] The first crystallization step results in nucleation and growth of polycrystalline α-Fe (the body-centered cubic phase, *bcc*, of Fe) nanograins surrounded by the residual amorphous matrix. The second step of crystallization leads to precipitation of additional crystalline (CR) phases along with the grain growth of all crystallites up to micrometer dimensions. Therefore, by varying the annealing conditions (time and temperature, below the temperature of the second crystallization) one alternates the fraction and size of the α-Fe nanograins. (iii) Among the Fe *M*B metallic glasses $Fe_{90}Zr_7B_3$ was selected because this particular ternary alloy contains the lowest amount of noniron atoms, only 10% of the sample composition. The main role of the Zr and B inclusions is to stabilize the initial amorphous state of the ribbon, to enhance its thermal stability, and to increase the nucleation rate during the nanocrystallization.[27] (iv) The crystallization kinetic of $Fe_{90}Zr_7B_3$ was studied in detail,[28] allowing for a reliable control over the crystallization process. (v) An established fitting model[29–31] to the Mössbauer spectra of this particular NC material offers the possibility to precisely determine (as described below) the relative fraction of resonant atoms (^{57}Fe) located inside the nanograins and at the interfaces. (vi) Finally, the internal formation of the nanocrystals in this bulk NC material prevents the nanoparticles from oxidation,

which very often takes place in NC samples synthesized by other methods. This, indeed, allows for ruling out the effects of oxidation on the vibrational thermodynamics of NC materials.

In this paper we determine, from the previously[25] obtained vibrational DOS, the lattice specific heat, vibrational entropy, mean atomic displacement, and mean-force constant of $Fe_{90}Zr_7B_3$ in as-quenched state and at various states of nanocrystallization. The carefully selected NC system allows to systematically investigate how the vibrational thermodynamics of the bulk NC materials is influenced by the amorphous, homogenous, and porosity-free interfaces. A direct comparison of the influence of the structural disorder with that of the broken translational symmetry at the surface on the thermoelastic properties of Fe is also presented and discussed.

II. EXPERIMENTAL AND THEORETICAL DETAILS

A. Samples preparation

An amorphous $Fe_{90}Zr_7B_3$ alloy, enriched to 63% in the resonant isotope ^{57}Fe, was produced by rapid quenching of the melt in vacuum by the single roller melt-spinning technique at a circumferential velocity of 37 m/s. NC samples with various stages of crystallization were prepared by isothermal annealing of the as-quenched 20 μm-thick ribbon in a vacuum (1.6×10^{-6} mbar) to avoid oxidation. The first $T_1=783(1)$ K and the second $T_2=1017(1)$ K crystallization temperatures were determined from the differential calorimetry scan (see Fig. 1). The following samples were studied (the abbreviation is the same as in our previous work[25]): *as-quenched*, *A*, *B*, *C*, and *D* standing for the amorphous precursor and the NC samples obtained by annealing of the precursor at 753 K for 10 min., 783 K for 10 min., 783 K for 30 min., and 893 K for 80 min., respectively. All samples were characterized by x-ray diffraction using Cu $K\alpha$ radiation [Fig. 1(a) from Ref. 25], and by conversion electron Mössbauer spectroscopy (CEMS). They confirmed the predominantly amorphous state of the as-quenched ribbon and excluded the presence of any kinds of oxides as well as any crystalline phases different from α-Fe in the NC samples. In agreement with earlier studies[32] on the same material nanograins of α-Fe with average sizes of about 2 nm and relative volume fraction of 16% were detected in the amorphous precursor by CEMS and by x-ray diffraction. The mean grain size d determined by Rietveld refinement of the x-ray diffractograms and by transmission electron microscopy, the calculated[33] mean intercrystalline layer thickness δ, and the relative atomic fraction of the intercrystalline phase X_{IC} in the studied samples are displayed in Table I.

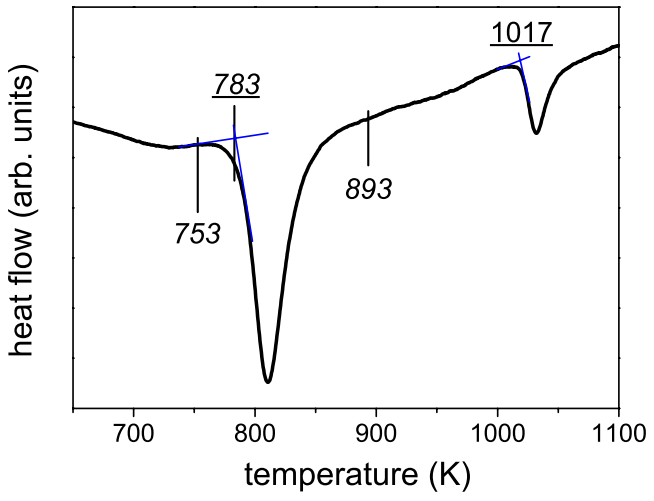

FIG. 1. (Color online) Differential-scanning calorimetry scan upon an amorphous $Fe_{90}Zr_7B_3$. The first and the second crystallization temperatures are shown (underlined numbers). The annealing temperatures at which the NC samples were obtained are also shown (italic numbers).

TABLE I. Mean size d of the α-Fe nanograins, mean intercrystalline layer thickness δ, and the corresponding atomic fraction X_{IC}.

Sample	d (nm)	δ (nm)	X_{IC}
as-quenched	2.2(5)	1.0(5)	0.84(2)
A	10.9(5)	2.3(5)	0.51(2)
B	12.5(5)	1.5(5)	0.32(2)
C	13.4(5)	1.0(5)	0.21(2)
D	14.9(5)	0.6(5)	0.11(2)

B. Conversion electron Mössbauer spectroscopy

The high sensitivity of Mössbauer spectroscopy to the local environment of the resonant nuclei allows one to identify the Fe atoms exhibiting different structural arrangements and to precisely determine their relative atomic fractions. Figure 2 displays the measured conversion electron Mössbauer spectra of all investigated samples at room temperature. According to an established fitting model[29,30] the Mössbauer spectra of this ternary NC alloy are composed of three different contributions. A narrow sextet (dotted line), characterized with a hyperfine field 33.0(1) T and an isomer shift −0.01(1)mm/s (relative to α-Fe), arises from the α-Fe nanograins. A broader sextet (dashed line), hyperfine field 31.8(1) T with a Gaussian distribution [width 3.7(1) T], and isomer shift −0.01(1)mm/s, originates from the atoms located at the (internal) surfaces of the nanograins with an average thickness of about 2 atomic layers. These atoms possess slightly reduced coordination number with respect to those of a perfect *bcc* crystal lattice. The third, quite broad component (filled gray area) is typical for a matter with high degree of structural disorder and it is assigned to the residual amorphous matrix, i.e., the intercrystalline phase. In the as-quenched sample this phase is nonmagnetic while in the nanocrystalline samples it is already in a ferromagnetic state with an average strength of the magnetic field 20 T and quite broad Gaussian distribution (width of about 10 T), induced by the interacting magnetic moments of the growing nanograins (polarization of the amorphous phase). Note that in sample *A* paramagnetic and ferromagnetic regions coexist within the intercrystalline material.

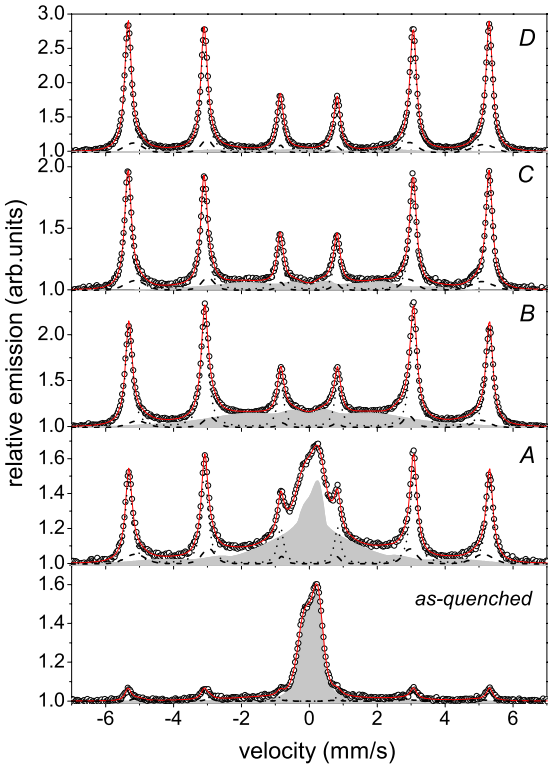

FIG. 2. (Color online) Conversion electron Mössbauer spectra (open circles) of the studied samples, decomposed to contributions from grains interior (dotted line), grains surface (dashed line), and intercrystalline fraction (filled gray area). The solid red lines mark the fits.

By applying this model the atomic fraction of the intercrystalline phase[34] X_{IC} (third component) is precisely separated from that of the nanograins and their surfaces (the first and second components) $1-X_{IC}$ (Table I). Upon annealing of the amorphous precursor one observes a gradual increase in the nanograin's fraction (Fig. 2, dotted line subspectrum) and simultaneous decrease in the intercrystalline phase (Fig. 2, gray area component). This behavior has also been confirmed by the x-ray diffraction data [Fig. 1(a) from Ref. 25].

C. Nuclear inelastic scattering

The nuclear inelastic scattering[35–37] experiments were performed at the Nuclear Resonance beamline ID18 (Ref. 38) of the European Synchrotron Radiation Facility (ESRF) employing a high-resolution monochromator with an energy bandwidth 1.0 meV.[39] The vibrational DOS of the as-quenched material, NC samples, and of a 8 μm thick α-Fe foil (95% enriched in ^{57}Fe) were derived in a quasiharmonic approximation from the probability for nuclear inelastic absorption measured in the energy range ± 70 meV at room temperature. Avalanche photodiode detectors[40] were used to detect the incoherent Fe $K\alpha$ fluorescence radiation (6.4 keV), emitted after de-excitation of the nuclear resonant level (14.4 keV) by internal conversion (conversion factor 8.2) with a time delay with respect to the moment of the phonon-assisted nuclear resonant absorption. In order to increase the count rate by covering larger solid angle with the detector the samples were inclined to an angle of only a few degrees with respect to the x-ray beam. This experimental geometry defined a depth sensitivity of approximately 1 μm, which is comparable with the surface sensitivity of the CEMS technique (about 0.2 μm). In addition, both CEMS and nuclear inelastic scattering experiments were performed on the same surface side of the ribbons. Therefore, both methods probed essentially the same part of the investigated samples, excluding errors due to a possible difference in the crystallization of the ribbons along their thickness. Furthermore, the isotopic selectivity of the nuclear resonance absorption and the applied experimental geometry ensured that the nuclear inelastic scattering and the Mössbauer spectroscopy probed the same atoms of the sample. Thanks to these conditions only one is able to reliably correlate the vibrational DOS with the atomic fraction of the nanograins and the intercrystalline material.

D. Theoretical considerations

In a nuclear inelastic scattering experiment one measures the energy dependence of the probability $W(E)$ for nuclear inelastic absorption while scanning the energy around the nuclear resonance energy in a millielectron-volt range employing a high-resolution monochromator.[41] After normalization, $W(E)$ is decomposed in terms of a multiphonon expansion[42]

$$W(E) = f_{LM}\left[\delta(E) + \sum_{1}^{\infty} S_n(E)\right], \tag{1}$$

where f_{LM} is the Lamb-Mössbauer factor, the Dirac function $\delta(E)$ describes the elastic part of absorption (zero-phonon term), and the nth term of the series $S_n(E)$ represents the inelastic absorption accompanied by creation and/or annihilation of n phonons. The one-phonon term is given by

$$S_1(E) = \frac{E_R g(E)}{E(1-e^{-\beta E})}. \tag{2}$$

$E_R = \frac{\hbar^2 k^2}{2M}$ is the recoil energy of a free nucleus, $\vec{k}$ is the wave vector of the photon; $\hbar$ is the reduced Planck constant; M is the atomic mass, E is the energy transfer, $\beta = (k_B T)^{-1}$, T is the temperature, k_B—the Boltzmann constant, and $g(E)$ is the density of vibrational states.

The only assumption involved in the data evaluation is the harmonic interaction between the atoms of the lattice. This allows one to apply the following recursive iteration:

$$S_n(E) = \frac{1}{n}\int_{-\infty}^{\infty} S_1(E') S_{n-1}(E-E')dE' \tag{3}$$

and to calculate $S_1(E)$ from the experimental data. The vibrational DOS $g(E)$ is obtained from Eq. (2).

By using the $g(E)$ a number of thermodynamic and elastic properties of a system can be calculated. For example, the vibrational entropy S_{vib} per atom is given by the expression

$$S_{vib} = 3k_B \int_0^\infty g(E) \left[\frac{\beta E}{2} \frac{e^{\beta E} + 1}{e^{\beta E} - 1} - \ln(e^{\beta E/2} - e^{-\beta E/2}) \right] dE. \tag{4}$$

The lattice specific heat per atom at constant volume C_V is defined as

$$C_V = 3k_B \int_0^\infty g(E) \frac{(\beta E)^2 e^{\beta E}}{(e^{\beta E} - 1)^2} dE. \tag{5}$$

The Lamb-Mössbauer factor and the mean-square atomic displacement can be also calculated

$$f_{LM} = \exp\left[- E_R \int_0^\infty \frac{g(E)}{E} \frac{1 + e^{-\beta E}}{1 - e^{-\beta E}} dE \right], \tag{6}$$

$$\langle \Delta x^2 \rangle = - \frac{\ln(f_{LM})}{k^2}. \tag{7}$$

The mean-force constant is given by

$$V = \frac{M}{\hbar^2} \int_0^\infty g(E) E^2 dE. \tag{8}$$

III. RESULTS AND DISCUSSIONS

A. Density of vibrational states

Figure 3 shows the iron-partial vibrational DOS (open circles) for all samples derived according to Eqs. (1)–(3). The partial contributions of the nanograin (dashed line) and the intercrystalline (dotted line) fractions are represented by the corresponding reference DOS functions [Fig. 2(b) from Ref. 25] weighted by their relative atomic fractions (Table I). The solid (red) lines mark the sum of two contributions. The total agreement between the open circles and the solid lines confirms that the applied decomposition of the vibrational DOS to contributions of nanograins and interfaces is fully consistent with the experimental data for all samples.

The vibrational DOS of the intercrystalline material is featureless exhibiting significant enhancement of vibrational states at low energy as well as a high-energy tail in comparison to that of bulk Fe (see Fig. 5). This particular DOS shape was obtained[25] from the vibrational DOS of the NC samples *A* and *C*. The fact that it is fully consistent with the DOS of the intercrystalline fraction in the as-quenched sample [Fig. 4(b) from Ref. 25], where 84% of the Fe atoms are in amorphous state, as confirmed by x-ray diffraction [Fig. 1(a) from Ref. 25], strongly suggests that the DOS of the intercrystalline material in the investigated NC samples is identical to that of amorphous Fe.

A comparison with the calculated[43] DOS of amorphous Fe reveals common features such as enhancement of vibrational states at low energy and broadening of the peaks. Some discrepancies, however, can also be observed, namely, the lack of a well-pronounced transverse excitation and the presence of a high-energy tail, not visible in the calculated vibrational spectrum.

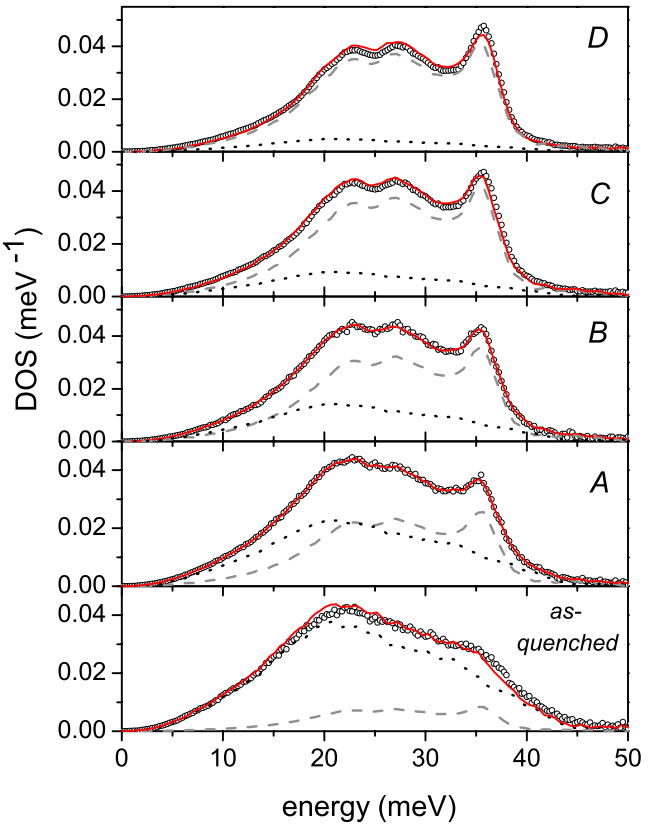

FIG. 3. (Color online) Fe-partial vibrational DOS (open circles) of the samples under study. The dashed and dotted lines represent the reference DOS functions of the nanograins and interfaces, respectively, derived as described in Ref. 25 and weighted by their relative atomic fractions. The red solid lines mark the sum of two contributions.

B. Thermodynamic and elastic properties

From the experimentally obtained vibrational DOS we calculated the thermodynamic and elastic properties of the NC alloy according to Eqs. (4)–(8). Figure 4 reveals the deviations (solid circles) of the (a) vibrational entropy $S_{vib.}$ per atom, (b) lattice specific heat C_V per atom, (c) mean atomic displacement, and (d) mean-force constant from the corresponding values of the bulk α-Fe as the intercrystalline amorphous fraction X_{IC} decreases upon annealing of the as-quenched precursor. These are, indeed, the reported anomalies in the vibrational thermodynamics of the NC materials. The open triangles at $X_{IC}=0.0$ and the open squares at $X_{IC}=1.0$ mark the calculated [Eqs. (4)–(8)] values by using the reference DOS of the nanograins and the intercrystalline fraction, respectively. The solid triangles at $X_{IC}=0.0$ denote the values related to bulk Fe obtained from the DOS of a polycrystalline α-Fe foil.

The values of the thermoelastic quantities of the nanograins are fairly close to those of the α-Fe foil (Fig. 4, open and solid triangles at $X_{IC}=0.0$) and practically coincide within the experimental error bars despite of the grain size variation between 2.0(5) nm in as-quenched sample and 14.9(5) nm in sample *D* (see Table I). This result is rather expected since the vibrational DOS of the nanograins is size

independent and almost identical to that of bulk α-Fe [Fig. 2(b) from Ref. 25]. The values at $X_{IC}=1.0$ (open squares) correspond to fully amorphous Fe and represent the limit for the deviations of the vibrational thermodynamic properties from those of crystalline Fe induced solely by the structural disorder (amorphous limit).

From the linear scaling of the low-energy enhancement of the vibrational DOS to the intercrystalline atomic fraction [Fig. 5(b) from Ref. 25] it directly follows that such linear scalings should also apply for the deviations of the thermoelastic properties from the corresponding bulk values. The solid red lines in Fig. 4 are linear fits to the data (solid circles) for the as-quenched, *A*, *B*, *C*, and *D* samples and, as expected, they perfectly follow the experimental points. The extrapolations to $X_{IC}=0.0$ and to $X_{IC}=1.0$ match, within the experimental error bars, the corresponding values of the nanograins and the intercrystalline fraction, respectively.

Similarly to the vibrational DOS (Fig. 3), a given thermodynamic property T_{NC} of the NC materials is a superposition of the corresponding property of the nanograins and the intercrystalline material weighted by their relative atomic fractions. Such decomposition of the vibrational thermodynamics of NC Ni suggested by Tang *et al.*,[45] revealed a linear scaling of the vibrational entropy and the lattice specific heat to the grain boundary fraction.

As demonstrated above, for the investigated NC samples the properties of the nanograins are very close to the properties (T_{CR}) of the coarse-grained crystalline counterpart (α-Fe) while the intercrystalline fraction is represented by the residual amorphous matrix (T_{AM}). Therefore, a certain thermodynamic property T_{NC} of this NC material is given by

$$T_{NC} = (1 - X_{IC})T_{CR} + X_{IC}T_{AM}. \quad (9)$$

As seen in Fig. 4 (open asterisks) this model satisfactorily reproduces the experimental values of the as-quenched, *A*, *B*, *C*, and *D* samples. We note, however, that this model holds only provided that the nanograins exhibit the same crystalline phase as the coarse-grained crystalline counterpart. Furthermore, presence of free volumes (voids and pores), oxides, other crystalline phases, or contaminations and impurities in the NC material will also result in deviations from Eq. (9).

Figure 4(a) reveals a variation in the vibrational entropy between $3.50(1)k_B$/atom($X_{IC}=1.0$) and $3.07(1)k_B$/atom($X_{IC}=0.0$) implying a maximal excess vibrational entropy $\Delta S_{vib.}$ for Fe of 0.43(1) k_B/atom, i.e., the decrease upon crystallization at room temperature is about 14%. This compares well with the reported[46] 15% increase in S_{vib} for amorphous relative to the crystalline $FeSi_2$. In addition, this trend is in agreement with the enhancement of the vibrational entropy by $0.30(1)k_B$/atom and by $0.10(3)k_B$/atom in disordered state compared to the ordered one for Ni_3Al (Ref. 47) and Fe_3Al,[48] respectively.

It is interesting to note that an enhancement of only $0.01k_B$/atom is obtained for NC Fe prepared by ballistic consolidation[4] while for NC Fe synthesized by ball milling[3] the value is by a factor of 2 larger, despite of the similar grain sizes in both samples (10 nm and 12 nm, respectively). On the other hand, our value $0.22(1)k_B$/atom for sample *A*

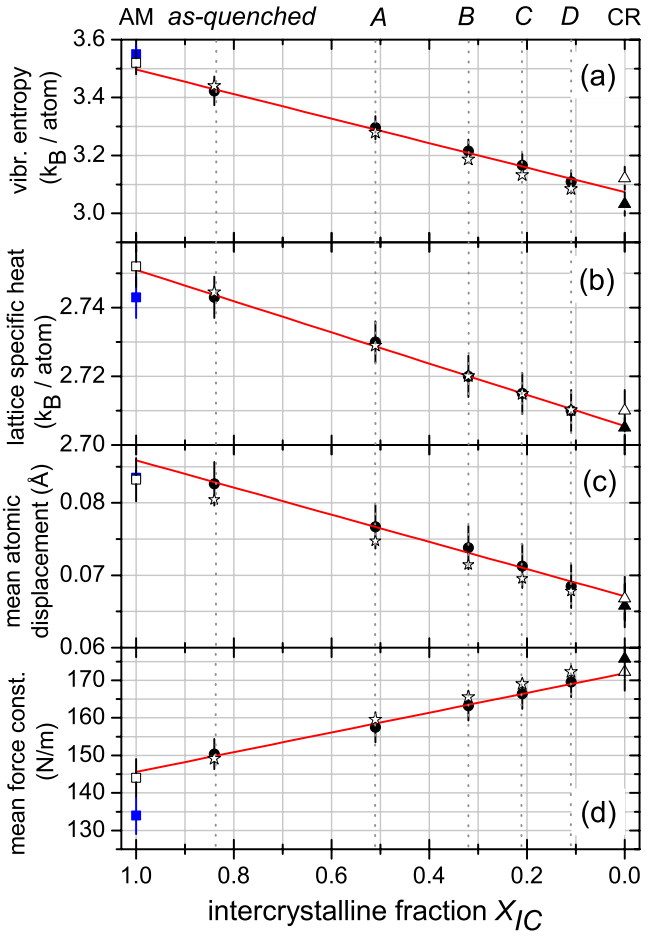

FIG. 4. (Color online)The room-temperature values of the (a) vibrational entropy, (b) lattice specific heat, (c) mean atomic displacement, and (d) mean-force constant of $Fe_{90}Zr_7B_3$ derived from the experimental DOS (Fig. 3) as a function of the intercrystalline fraction X_{IC}. The open squares at $X_{IC}=1.0$ and the open triangles at $X_{IC}=0.0$ denote the values calculated from the reference vibrational DOS (Ref. 25) of the intercrystalline and the nanograin fractions marked as AM and CR, respectively. The solid triangles mark the corresponding values of α-Fe foil. The solid red lines are linear fits to the experimental points of samples as-quenched, *A*, *B*, *C*, and *D* (solid circles). Open asterisks mark the values calculated by Eq. (9). The solid (blue) squares at $X_{IC}=1.0$ denote the mean values of a clean Fe(110) surface (Ref. 44) (see text).

(grain size 11 nm) is fully consistent with the calculated[8] $0.215k_B$/atom for NC α-^{57}Fe with 10 nm grain size. These discrepancies demonstrate that the properties of NC materials synthesized by different techniques have to be compared with caution since the resulting interfaces, mainly responsible for the observed anomalies, could significantly differ by their fraction, density, and degree of structural disorder.

The lattice specific heat [Fig. 4(b)] decreases upon crystallization from $2.75(1)k_B$/atom($X_{IC}=1.0$) to $2.71(1)$ k_B/atom($X_{IC}=0.0$), i.e., by 1.5% only. This value is consistent with the reported difference of 2.7% between amorphous and crystalline $FeSi_2$.[46] In addition, it is in good agreement with the specific-heat enhancement of 2% found for amorphous and NC Se relative to the coarse-grained polycrystalline Se (Ref. 9) as well as with the increase in 3% measured

in NC Ni.[10] The results presented here demonstrate that the structural disorder of the interfaces has a minor contribution to the anomalous behavior of the lattice specific heat of NC materials. Sample *C*, for example, characterized with X_{IC} =0.21, mean grain size 13.4(5) nm and intercrystalline layer thickness of 1.0(5) nm (typical value for the NC interface thickness regardless of the synthesizing method), reveals an increase in only 0.18% compared to the bulk value. The specific-heat enhancements of up to 40% (Ref. 11) reported in literature are most likely the result of contamination and impurities of the NC samples and it is not related to the disordered interfaces. As demonstrated[13] by Tschöpe and Birringer such contaminations could significantly influence the specific heat of the NC materials.

The mean atomic displacement, i.e., the square root of the mean-square atomic displacement, [Fig. 4(c)] changes its value between 0.084(1) Å(X_{IC}=1.0) and 0.066 (1) Å(X_{IC}=0.0) implying a decrease in about 27% upon crystallization. The corresponding values for samples *B* and *C* are 9.8% and 6.3%, respectively while for sample *D* it is 2.7%. They are in good agreement with the calculated[49] mean-square displacements of nanocrystalline Au, Ag, and Al employing the Lindemann theory of melting.[50] The calculated deviation of about 30% found for NC Ag (2 nm particles size) is consistent with the 25% enhancement derived for the as-quenched sample (grain size 2 nm).

Figure 4(d) reveals a variation in the mean-force constant between 145 N/m(X_{IC}=1.0) and 172 N/m(X_{IC}=0.0) indicating a decrease by about 16% upon crystallization. Again, this value is fully consistent with the reported[46] difference of 17% between the mean-force constants in crystalline and in amorphous $FeSi_2$. The systematic decrease in the mean force constant in the NC samples with larger fraction of disordered interfaces leads to a lower sound velocity, which manifests itself as an enhancement of the vibrational DOS in the low-energy range in comparison to that of the bulk counterparts. This has experimentally been observed and depicted on Fig. 5(b) of Ref. 25.

Finally, we compare the influence of the structural disorder with that of the broken translational symmetry at the surface on the thermoelastic properties of Fe. Recent instrumentation developments[51] at the beamline ID18 of the ESRF allowed for *in situ* studies of the vibrational properties of ultrathin Fe films, and to investigate effects of the reduced coordination at the surface[44] and the substrate-induced strain[52] on the lattice dynamics of Fe monolayers. The solid (blue) squares at X_{IC}=1.0 on Fig. 4 denote the corresponding average values obtained from the DOS of a clean Fe(110) surface with the wave vector of the x-rays being parallel to the [001] and [1$\bar{1}$0] crystallographic directions.[44] The data plotted on Fig. 4 demonstrate that the vibrational entropy and the mean atomic displacement of amorphous Fe practically coincide with that of a clean Fe(110) surface. Although the lattice specific heat and the mean force constant for the Fe(110) surface are slightly lower compared to the corresponding values of amorphous Fe, they still coincide within the experimental error bars. This comparison reveals that the vibrational thermodynamics is influenced practically in the same manner from the structural disorder as from the broken translational symmetry at the surface.

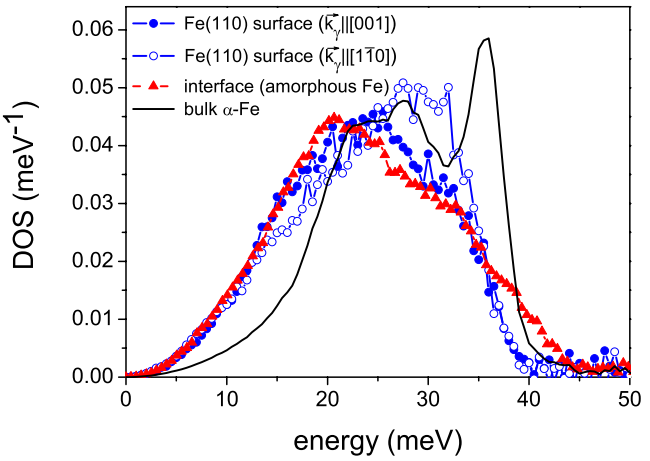

FIG. 5. (Color online) A comparison of the interface DOS (solid red triangles) (from Ref. 25), with that of the Fe(110) surface obtained with the wave vector of the photons being parallel to the [001] (solid circles) and to the [1$\bar{1}$0] (open blue circles) crystallographic directions (from Ref. 44). The solid black line represents the DOS of the bulk α-Fe.

To get more insight into this phenomenon we plotted on Fig. 5 the reference DOS of the intercrystalline fraction (solid red triangles) and of the Fe(110) surface obtained with the wave vector of the incoming photons parallel to [001] (solid blue circles) and to [1$\bar{1}$0] (open blue circles) crystallographic directions.[44] For comparison the DOS of bulk α-Fe is also shown with solid line.

Figure 5 surprisingly reveals that the vibrational spectrum of the intercrystalline fraction (amorphous Fe) exhibits similar features to the surface DOS such as enhancement of states at low energies and suppression of the high-energy phonon mode. In particular, the enhancement of vibrational states at low energies, i.e., between 0 and 14 meV, is practically the same for the surface and the interface DOS. The main differences are visible in the range between 25 and 35 meV, where the DOS of the Fe surface shows an excess of vibrational states compared to the DOS of the intercrystalline material. Above 35 meV the intercrystalline DOS posses a high-energy tail up to about 45 meV while the surface DOS exhibits a high-energy cutoff slightly lower compared to that of bulk α-Fe. As a result the vibrational DOS of the surface has similar anomalous features to that of the intercrystalline fraction leading to very close values of the corresponding thermoelastic properties, as demonstrated on Fig. 4.

IV. CONCLUSIONS

The room-temperature thermodynamic (lattice specific heat, vibrational entropy) and elastic (mean-force constants, mean atomic displacement) properties of $Fe_{90}Zr_7B_3$ were determined in as-quenched and in various nanocrystalline states from the previously[25] measured iron-partial density of vibrational states. The analysis revealed that the transformation of the Nanoperm alloy from amorphous to crystalline through various nanocrystalline states leads to a gradual decrease in the vibrational entropy, lattice specific heat, and mean atomic

displacement by 14%, 1.5%, and 27%, respectively, while the mean-force constant increases by 16%. The thermoelastic properties of this NC alloy are represented as a linear combination of the corresponding property of the material in crystalline and in amorphous states weighted by the relative atomic fractions of the nanograins and the intercrystalline material, respectively. This applies for NC materials obtained by crystallization of an amorphous precursor in general, provided that the nanocrystalline fraction exhibits the same crystalline phase as the coarse-grained counterpart, and no other phases, oxides, and impurities are present.

A direct comparison with the vibrational thermodynamics of a clean Fe surface revealed that the broken translational symmetry at the surface influences the thermoelastic properties in practically the same manner as the structural disorder does. This is a consequence of the very similar anomalous enhancements of vibrational states at low energy exhibited by the corresponding vibrational DOS and being primarily responsible for the observed anomalies.

ACKNOWLEDGMENTS

S.S. acknowledges the support by the Helmholtz Association (VHNG-625). M.M. acknowledges the support by VEGA under Grants No. 1/0033/10 and No. MSM6198959218. This work was partly supported by the Austrian FWF under Project No. P-20767-N20.

*svetoslav.stankov@kit.edu

[1] B. Fultz, Prog. Mater. Sci. **55**, 247 (2010).
[2] C. Suryanarayana and C. C. Koch, Hyperfine Interact. **130**, 5 (2000).
[3] B. Fultz, J. L. Robertson, T. A. Stephens, L. J. Nagel, and S. Spooner, J. Appl. Phys. **79**, 8318 (1996).
[4] B. Fultz, C. C. Ahn, E. E. Alp, W. Sturhahn, and T. S. Toellner, Phys. Rev. Lett. **79**, 937 (1997).
[5] H. N. Frase, L. J. Nagel, J. L. Robertson, and B. Fultz, Philos. Mag. B **75**, 335 (1997).
[6] H. Frase, B. Fultz, and J. L. Robertson, Phys. Rev. B **57**, 898 (1998).
[7] A. Kara and T. S. Rahman, Phys. Rev. Lett. **81**, 1453 (1998).
[8] R. Singh, S. Prakash, and J. Chinese, Physica **40**, 624 (2002).
[9] N. X. Sun and K. Lu, Phys. Rev. B **54**, 6058 (1996).
[10] L. Wang, Z. Tan, S. Meng, D. Liang, and B. Liu, Thermochim. Acta **386**, 23 (2002).
[11] J. Rupp and R. Birringer, Phys. Rev. B **36**, 7888 (1987).
[12] E. Hellstern, H. J. Fecht, Z. Fu, and W. L. Johnson, J. Appl. Phys. **65**, 305 (1989).
[13] A. Tschöpe and R. Birringer, Philos. Mag. B **68**, 223 (1993).
[14] D. Wolf, J. Wang, S. R. Phillpot, and H. Gleiter, Phys. Rev. Lett. **74**, 4686 (1995).
[15] J. Trampenau, K. Bauszus, W. Petry, and U. Herr, Nanostruct. Mater. **6**, 551 (1995).
[16] U. Stuhr, H. Wipf, K. H. Andersen, and H. Hahn, Phys. Rev. Lett. **81**, 1449 (1998).
[17] R. Röhlsberger, W. Sturhahn, T. S. Toellner, K. W. Quast, P. Hession, M. Hu, J. Sutter, and E. E. Alp, J. Appl. Phys. **86**, 584 (1999).
[18] E. Bonetti, L. Pasquini, E. Sampaolesi, A. Deriu, and G. Cicognani, J. Appl. Phys. **88**, 4571 (2000).
[19] L. Pasquini, A. Barla, A. I. Chumakov, O. Leupold, R. Rüffer, A. Deriu, and E. Bonetti, Phys. Rev. B **66**, 073410 (2002).
[20] A. F. Yue, A. B. Papandrew, O. Delaire, B. Fultz, Z. Chowdhuri, R. M. Dimeo, and D. A. Neumann, Phys. Rev. Lett. **93**, 205501 (2004).
[21] B. Roldan Cuenya, A. Naitabdi, J. Croy, W. Sturhahn, J. Y. Zhao, E. E. Alp, R. Meyer, D. Sudfeld, E. Schuster, and W. Keune, Phys. Rev. B **76**, 195422 (2007).
[22] C. Hudon, R. Meyer, and L. J. Lewis, Phys. Rev. B **76**, 045409 (2007).
[23] B. Roldan Cuenya, L. K. Ono, J. R. Croy, A. Naitabdi, H. Heinrich, J. Zhao, E. E. Alp, W. Sturhahn, and W. Keune, Appl. Phys. Lett. **95**, 143103 (2009).
[24] B. Roldan Cuenya, J. R. Croy, L. K. Ono, A. Naitabdi, H. Heinrich, W. Keune, J. Zhao, W. Sturhahn, E. E. Alp, and M. Hu, Phys. Rev. B **80**, 125412 (2009).
[25] S. Stankov, Y. Z. Yue, M. Miglierini, B. Sepiol, I. Sergueev, A. I. Chumakov, L. Hu, P. Svec, and R. Rüffer, Phys. Rev. Lett. **100**, 235503 (2008).
[26] M. E. McHenry, F. Johnson, H. Okumura, T. Ohkubo, V. R. V. Ramanan, and D. E. Laughlin, Scr. Mater. **48**, 881 (2003).
[27] K. Suzuki, Mater. Sci. Forum **312-314**, 521 (1999).
[28] K. Suzuki, J. M. Cadogan, V. Sahajwalla, A. Inoue, and T. Masumoto, Mater. Sci. Forum **235-238**, 765 (1997).
[29] M. Miglierini and J. M. Grenèche, J. Phys.: Condens. Matter **9**, 2303 (1997).
[30] M. Miglierini and J. M. Grenèche, J. Phys.: Condens. Matter **9**, 2321 (1997).
[31] S. Stankov, B. Sepiol, T. Kanuch, D. Scherjau, R. Würschum, and M. Miglierini, J. Phys.: Condens. Matter **17**, 3183 (2005).
[32] T. Ohkubo, H. Kai, A. Makino, and Y. Hirotsu, Mater. Sci. Eng., A **312**, 274 (2001).
[33] G. Palumbo, S. J. Thorpe, and K. Aust, Scr. Metall. Mater. **24**, 1347 (1990).
[34] Because both "interface" and "intercrystalline fraction" refer to one and the same component of the sample, i.e., the material in between the nanograins, hereafter the latter only is used to avoid confusions.
[35] M. Seto, Y. Yoda, S. Kikuta, X. W. Zhang, and M. Ando, Phys. Rev. Lett. **74**, 3828 (1995).
[36] W. Sturhahn, T. S. Toellner, E. E. Alp, X. Zhang, M. Ando, Y. Yoda, S. Kikuta, M. Seto, C. W. Kimball, and B. Dabrowski, Phys. Rev. Lett. **74**, 3832 (1995).
[37] A. I. Chumakov, R. Rüffer, H. Grünsteudel, H. F. Grünsteudel, G. Grübel, J. Metge, O. Leupold, and H. A. Goodwin, Europhys. Lett. **30**, 427 (1995).
[38] R. Rüffer and A. I. Chumakov, Hyperfine Interact. **97-98**, 589 (1996).
[39] A. I. Chumakov (unpublished).
[40] A. Q. R. Baron, R. Rüffer, and J. Metge, Nucl. Instrum. Methods

Phys. Res. A **400**, 124 (1997).
[41] R. Röhlsberger, *Nuclear Condensed Matter Physics with Synchrotron Radiation* (Springer-Verlag, Berlin, 2004).
[42] K. Singwi and A. Sjölander, Phys. Rev. **120**, 1093 (1960).
[43] R. Yamamoto, K. Haga, T. Mihara, M. Doyama, J. Phys. F: Met. Phys. **10**, 1389 (1980).
[44] T. Ślęzak, J. Łażewski, S. Stankov, K. Parlinski, R. Reitinger, M. Rennhofer, R. Rüffer, B. Sepiol, M. Ślęzak, N. Spiridis, M. Zając, A. I. Chumakov, and J. Korecki, Phys. Rev. Lett. **99**, 066103 (2007).
[45] J.-F. Tang, X.-S. Li, W.-Y. Long, and Y. Wang, Phys. Status Solidi B **245**, 1527 (2008).
[46] M. Walterfang, W. Keune, E. Schuster, A. T. Zayak, P. Entel, W. Sturhahn, T. S. Toellner, E. E. Alp, P. T. Jochym, and K. Parliński, Phys. Rev. B **71**, 035309 (2005).
[47] L. Anthony, J. K. Okamoto, and B. Fultz, Phys. Rev. Lett. **70**, 1128 (1993).
[48] L. Anthony, L. J. Nagel, J. K. Okamoto, and B. Fultz, Phys. Rev. Lett. **73**, 3034 (1994).
[49] K. Sadaiyandi, Mater. Chem. Phys. **115**, 703 (2009).
[50] F. Lindemann, Phys. Z. **11**, 609 (1910).
[51] S. Stankov, R. Rüffer, M. Sladecek, M. Rennhofer, B. Sepiol, G. Vogl, N. Spiridis, T. Ślezak, and J. Korecki, Rev. Sci. Instrum. **79**, 045108 (2008).
[52] S. Stankov, R. Röhlsberger, T. Ślezak, M. Sladecek, B. Sepiol, G. Vogl, A. I. Chumakov, R. Rüffer, N. Spiridis, J. Łażewski, K. Parliński, and J. Korecki, Phys. Rev. Lett. **99**, 185501 (2007).